Molecular Crystals and Liquid Crystals
Publication details, including instructions for authors and subscription information:
http://www.tandfonline.com/loi/gmcl20

Quantum Transport in μ-Cyclopentadienyl Indium Complex

Yukihito Matsuura [a] & Toshifumi Morioka [a]
[a] Department of Chemical Engineering , Nara National College of Technology, 22 Yatacho, Yamato-Koriyama , Nara , Japan
Published online: 02 Apr 2013.

To cite this article: Yukihito Matsuura & Toshifumi Morioka (2013) Quantum Transport in μ-Cyclopentadienyl Indium Complex, Molecular Crystals and Liquid Crystals, 574:1, 135-142, DOI: 10.1080/15421406.2012.763016

To link to this article: http://dx.doi.org/10.1080/15421406.2012.763016

Mol. Cryst. Liq. Cryst., Vol. 574: pp. 135–142, 2013

ISSN: 1542-1406 print/1563-5287 online
DOI: 10.1080/15421406.2012.763016

Taylor & Francis
Taylor & Francis Group

Quantum Transport in μ-Cyclopentadienyl Indium Complex

YUKIHITO MATSUURA* AND TOSHIFUMI MORIOKA

Department of Chemical Engineering, Nara National College of Technology, 22 Yatacho, Yamato-Koriyama, Nara, Japan

The electronic structure and conductance of a μ-cyclopentadienyl indium (Cp–In) multidecker complex have been examined by using the density functional theory (DFT). The electrical conduction of the complex between gold electrodes is investigated by using Green's function formalism. The one-dimensional band structure exhibited semiconducting properties. The $Cp_5In_4^-$ complex, which had a long molecular length, between gold electrodes, exhibited low electrical conduction. On the other hand, the $Cp_3In_2^-$ complex between the gold electrodes had transmission at the Fermi level. The I–V curves suggest the intrinsic characteristics of semiconducting properties and the suppression of strong tunneling effect.

Keywords Cyclopentadienyl-indium complex; DFT; quantum transport

1. Introduction

In the near future, conventional silicon-based microelectronics is likely to reach its limit of miniaturization imposed by the laws of physics. Electron transport through molecular-scale devices has attracted considerable attention in experimental fields [1]. Aviram and Ratner have proposed a molecular diode that has the same functionality as semiconductor devices [2]. Recent theoretical studies have developed first-principle Green's function formalism with density functional theory (DFT) and have focused on the rectifying properties of molecules connected to metal electrodes [3,4].

In general, molecules attached to a metal electrode provide a different electronic state from the isolated state. Therefore, it is important to consider the junction between the molecule and the metal surface. It is well known that among these compounds, aromatic compounds such as benzene and cyclopentadienyl (Cp) ring energetically prefer to be adsorbed on a Pt(111) surface [5]. Therefore, it is also assumed that the Cp ring at the end of Cp-metal atom multidecker sandwich complexes can be stabilized on a Pt(111) surface. Previously, we studied the electronic structure of a Cp–In multidecker sandwich complex adsorbed on a Pt slab and clarified that the complex was energetically stabilized by weakening the antibonding state of the C–In bond in the complex [6].

Recently, electron transport in Cp-transition metal atom multidecker complexes has attracted attention in the field of molecular electronic devices [7]. These are expected

*Address correspondence to Yukihito Matsuura, Department of Chemical Engineering, Nara National College of Technology, 22 Yatacho, Yamato-Koriyama, Nara 639-1080, Japan. E-mail: matsuura@chem.nara-k.ac.jp

to be applied for use in magnetic tunneling devices, that is, spintronics. For example, Cp–Fe or Cp–Ni multidecker sandwich complexes were predicted to exhibit half-metallic properties with spin-filtering efficiency [8]. Cp-typical element complexes have also been synthesized extensively [9]. However, the electrical conduction of the complex between the metal electrodes has not been investigated experimentally or theoretically. Especially, Cp–In or Cp–thallium multidecker sandwich complexes have a zigzag structure in which the In–In–In angle is about 130°–140°. In this study, we have focused on the electron transport in the Cp–In multidecker sandwich complexes between the two gold electrodes by using Green's function formalism with a DFT approach. For reference, we have also optimized the structure of a polymeric Cp–In multidecker complex and have calculated the band structure with the DFT approach.

2. Computational Method

To obtain the electronic structure and relaxed atomic positions from the DFT, we have used the Atomistix Toolkit 2010.8.2, which is based on the SIESTA code, as the DFT platform [10,11,12]. In the DFT calculation, we employ the local density approximation (LDA) pseudo-potential for exchange correlation. A single-ζ plus polarization basis set was adopted for all the atoms. The mesh cutoff was set at 75 Ry in the calculation. The geometry optimization is carried out by conjugate gradient relaxation until the forces are smaller than 0.05 eVÅ^{-1}.

The one-dimensional band calculation of the polymeric Cp–In complex was carried out using the DFT method. In the polymeric system, the unit cell of the polymeric Cp–In complex consists of two In atoms and two Cp rings, as shown in Fig. 1(a). Twenty representative wave vectors (k) were chosen from G(000) to Z(001) with regular intervals.

Subsequently, we constructed a model of a $Cp_5In_4^-$ and $Cp_3In_2^-$ complex between the two gold electrodes, as shown in Figs. 1(b) and (c), respectively. In the complexes, all the Cp rings have 6π electrons. Although these complexes are anions, our previous studies suggest that the complexes are stabilized on the metal electrodes [6]. The bond length of the Au–Au bond of the face-centred cubic Au crystal was taken from a default value of 2.88 Å in the program package. To calculate the electron transport, we constructed a scattering region that included the complex (molecular region) and the three gold layers with a lateral (4×5) supercell as part of the electrodes. The Cp rings at the end of the complex are attached to the left and right (111) surfaces of the three gold layers in the scattering region, as shown in Figs. 1(b) and (c). The coordinates of the gold atoms in the molecular region are fixed, whereas those of the other atoms are fully optimized.

The electron transport calculations were carried out using the program based on nonequilibrium Green's function with the DFT approach [12]. The transmittance ($T(E,V)$) at the energy E under the bias V was calculated from the Landauer formula:

$$T(E,\ V) = Tr[G_L G \Gamma_R G^+],$$

where Γ_i (i = L, R), G, and G^+ are the coupling strengths that are calculated from the self-energies of the left and right electrodes (i = L, R), the retarded Green's function of the scattering region, and the advanced Green's function of the scattering region, respectively. Subsequently, the conductance ($G(E,\ V)$) is calculated as follows:

$$G(E,\ V) = 2e^2/hT(E,\ V).$$

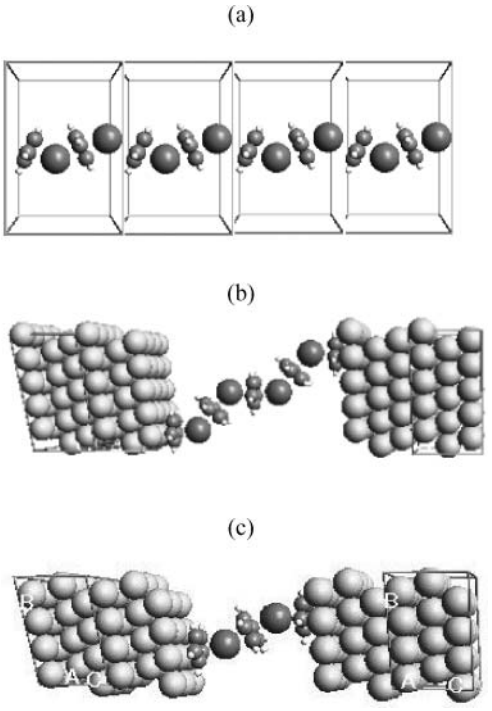

Figure 1. Configuration of (a) Cp_2In_2 as a unit cell of the polymeric Cp–In complex, (b) $Cp_5In_4^-$ complex between the gold electrodes, and (c) $Cp_3In_2^-$ complex between the gold electrodes. A rectangular parallelepiped indicates a periodic Cp_2In_2.

Finally, we can obtain the current ($I(V)$) under the bias V from the following equation:

$$I(V) = \int_{-\infty}^{\infty} dE\, T(E, V)[n_p(E - \mu_L) - n_p(E - \mu_R)],$$

where $n_F(E\text{-}\mu_L)$ is the Fermi–Dirac distribution of the system with the chemical potential μ_L.

3. Results and Discussion

3.1 Band Structure of the Polymeric Cp–In Complex

We first calculated the band structure of the polymeric Cp–In complex using the DFT method. The configuration of a unit cell of Cp_2In_2 is shown in Fig. 1(a). The shape of the Cp ring is almost a regular pentagon in which the C–C bond length is 1.44 Å. The length of the C–In bond ranges from 2.88 Å to 2.92 Å, suggesting that the vector of the neighboring In atoms is not perpendicular to the Cp ring. The length of the Cp–In is 2.63 Å, which is within the range of 2.50 Å to 2.69 Å, as shown in the experimental results of reference [9]. The In–In–In angle of 135° is a little bigger than that of the experimental results of 128°–134° [9].

Figure 2 indicates the band structure and the total density of states (DOS) of polymeric complex. The electronic structure is a semiconductor whose direct band gap is 2.88 eV.

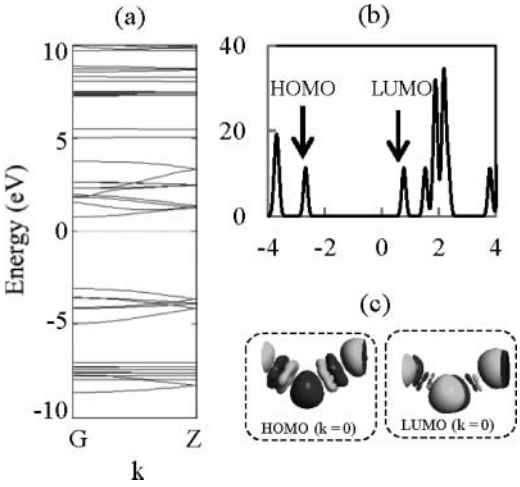

Figure 2. (a) Band structure and (b) total DOS of polymeric Cp–In complex. (c) The HOMO and LUMO at $k = 0$ are also described.

The highest occupied molecular orbital (HOMO) at $k = 0$ consists of an antibonding state between the In 5s orbital and the Cp a_1 orbital with a small contribution of the In 5p orbital. The phase patterns suggest the delocalization of the electrons at energy levels of the HO band. The HOMO – 1 and HOMO – 2 at $k = 0$ are the degenerated localized states formed by the Cp e_1 orbitals with a very small contribution of the In atomic orbitals. The LUMO and LUMO + 1 consist primarily of the In $5p_x$ and $5p_y$ orbitals, respectively. The band structure at the energy level around the Fermi level possesses the same tendency as that reported in references [6, 13, 14].

3.2 Electron Transport of $Cp_5In_4^-$ Complex between Gold Electrodes

We mention the configuration of the $Cp_5In_4^-$ complex between the two gold electrodes. The optimized configuration of the unit cell had a zigzag-staggered form, as shown in Fig. 1(b). The shape of the Cp ring is almost a regular pentagon, in which the C–C bond length at the end of the complex is 1.44 Å–1.45 Å and that at the central Cp ring is 1.43 Å. The bond length of the C–H bond is 1.16 Å–1.17 Å. The dihedral angles of C–C–C–H in the Cp ring are 176°–179°, in which the hydrogen atoms bend away slightly from the Au(111) surface. The lengths of the C–In bond attached to the carbon atom at the end are 2.81 Å–3.10 Å, and the length of that attached to the carbon atoms at the central Cp ring is 2.91 Å–2.96 Å. Although it has a larger value than that of the optimized polymeric structure of 2.63 Å, the Cp–In distance of 2.67 Å is within the range of the experimental results [9]. The In–In–In angle is 138°, and the nearest C–Au length is 2.90 Å. The plane of the Cp ring is almost parallel to the Au(111) surface. A centre of gravity of Cp ring is located in the vertical direction of the hollow site of the Au(111) surface.

Next, we will show the result of the transmission of $Cp_5In_4^-$ complex between gold electrodes, as shown in Fig. 3(a). The HOMO and LUMO of the molecular-projected self-consistent Hamiltonian (MPSH) are located at −2.02 eV and 1.83 eV. As in the polymeric Cp–In complex, the HOMO consists of In 5s orbital combined with Cp a_1 orbital as an anti-bonding state. The LUMO was constructed by Cp e_1 orbitals. There is very little transmission at the energy levels ranging from −2.0 eV to 1.8 eV, which suggests that

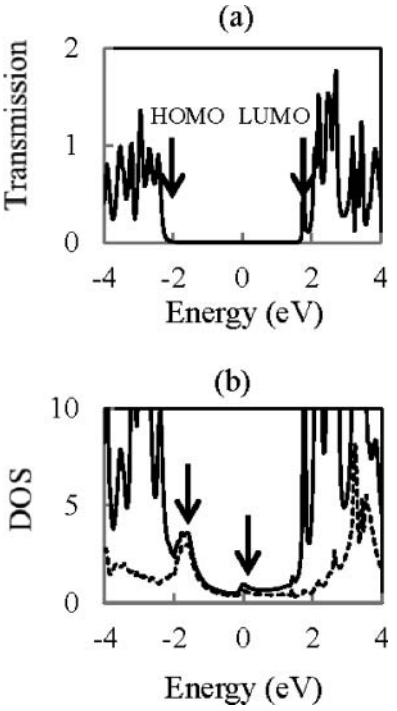

Figure 3. (a) Transmission spectrum of $Cp_5In_4^-$ complex between the gold electrodes under a bias of 0 V. The arrows indicate the energy level of HOMO and LUMO of MPSH. (b) DOS and PDOS for C 2p orbitals at the end of the complex (solid line: total DOS, dotted line: PDOS for C 2p orbital). The arrows indicate remarkable peaks between the HOMO–LUMO gap.

electrical conduction cannot be expected. As a result, the conduction of the complex is a very small value of 1.7×10^{-3} μS. Figure 3(b) indicates the total DOS and projected DOS for C 2p orbitals at the end of the complex. Compared to the transmission in Fig. 3(a), we can observe two peaks, which are indicated by two arrows in Fig. 3(b), with a wide range of intensity of DOS from -2 eV to 2 eV. From the plot of the dotted line in Fig. 3(b), we can conclude that the intensity of the DOS is primarily dependent on the C 2p orbitals at the end of the complex. This result suggests that the localized electrons on the Cp ring at the end of the complex do not contribute to the electrical conduction because of the long distance between the left and right electrodes.

3.3 Electron Transport of $Cp_3In_2^-$ Complex between Gold Electrodes

Since the optimized structure of the $Cp_3In_2^-$ complex had the same tendency as the Cp_5In_4 complex, the details will not be mentioned here. Figure 4(a) shows the transmission spectrum of the $Cp_3In_2^-$ complex between the gold electrodes. There are wide ranges of transmission from -3.5 eV to -1.5 eV and from 2.5 eV to 3.5 eV. Additionally, there is a small peak at the Fermi level. In general, since the conductance at zero bias is dependent on the transmission at the Fermi energy, this complex can exhibit electrical conduction of 5.5 μS.

We also examined the origin of the electrical conduction by calculating the MPSH. As shown in Fig. 4, the HOMO at -1.86 eV consists primarily of In 5s orbitals and Cp

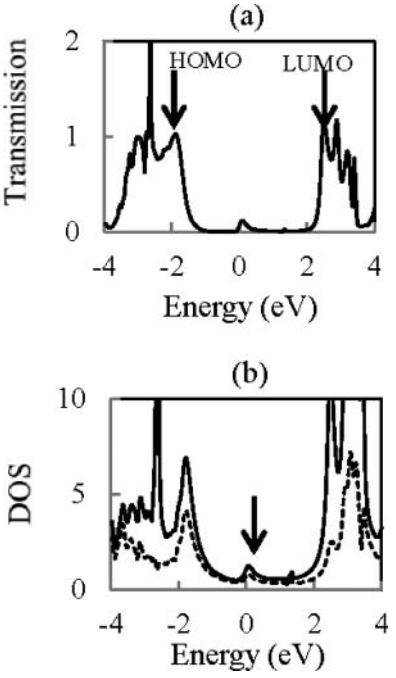

Figure 4. (a) Transmission spectrum of $Cp_3In_2^-$ complex between the gold electrodes under a bias of 0 V. The arrows indicate the energy level of HOMO and LUMO of MPSH. (b) DOS and PDOS for C 2p orbitals at the end of the complex (solid line: total DOS, dotted line: PDOS for C 2p orbital). The arrow indicates a remarkable peak at the Femi level.

a_1 orbitals, and the LUMO at 2.45 eV includes In 5p orbitals, whose phase patterns are similar to those of the polymeric Cp–In complex, as mentioned in Fig. 2 and in references [6,13,14]. The MPSH state projected on the molecular region had no energy level around the Fermi level in the transmission (Fig. 4(a)) and the DOS plots (Fig. 4(b)). However, there is a sharp peak as a gap state at the Fermi level. The MPSH state calculated by including the gold electrode suggests that the electron density is primarily concentrated on the gold surfaces and the Cp 2p orbitals at the end of the complex. The MPSH analysis is also confirmed by the result of the total DOS and the PDOS at the molecular region. Figure 4(b) suggests that the transmission is determined almost entirely by the total DOS. To analyze in more detail, we analyzed the PDOS for the C 2p orbital at the end of the complex. The dotted line suggests that the transmission at the Fermi level is dependent on the C 2p orbitals at the end of the complex. Since the length of the complex is short, weak tunneling effect takes place due to the states of electrodes and the end of the complex.

3.4 Bias-Dependence of the Electron Transport of Cp–In Complex between Gold Electrodes

We examined the dependence of the electrical conduction of the $Cp_3In_2^-$ complex between the gold electrodes on the bias voltage. The configuration optimized under a bias voltage of 0 V was used for these calculations because of our computational limit. Figure 5 shows a plot of the current in the molecular region against the bias voltage between the two gold electrodes. Since this complex has a symmetric structure, we examined currents and

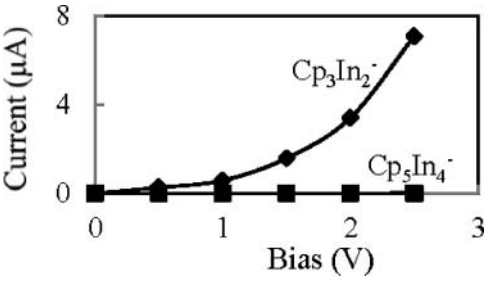

Figure 5. Current–bias characteristic of $Cp_3In_2^-$ and $Cp_5In_4^-$ complex between the gold electrodes.

conductance in a range from 0 V to 2.5 V. The current did not increase readily with the applied bias due to suppression of a strong tunneling effect, as in a case of a long silicon nanowire [15]. To examine the results in more detail, we calculated the electron transport and the PDOS when the bias increased.

The electron transports at bias voltages of 1.0 V and 2.0 V are shown in Figs. 6(a) and (b). As the bias increases, the transmission peak at the Fermi level at zero bias is shifted to the high energy level (peaks of 0.542 eV and 1.025 eV at bias voltages of 1.0 V and 2.0 V, respectively) and becomes very small. The energy levels around the Fermi level at

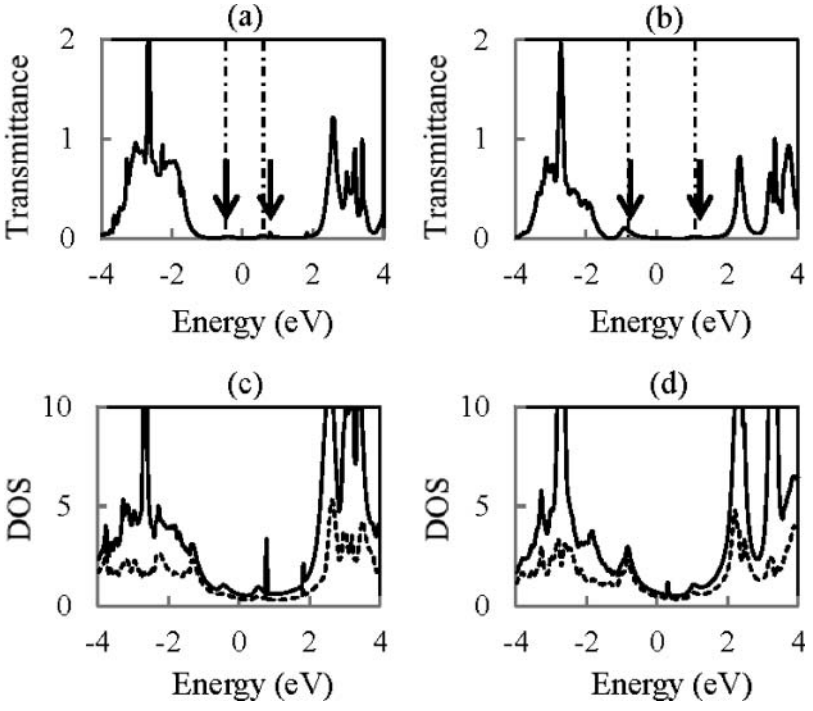

Figure 6. Transmission spectra under biases of (a) 1.0 V and (b) 2.0 V of $Cp_3In_2^-$ complex between the gold electrodes. The arrows indicate remarkable peaks. Total DOS and PDOS for C 2p orbitals at the end of $Cp_3In_2^-$ complex between the gold electrodes. (solid line: total DOS, dotted line: PDOS for C 2p orbital) under biases of (c) 1.0 V and (d) 2.0 V. Dashed lines in (a) and (b) indicate the bias window.

zero bias, whose MPSH was located at the left electrode, were raised by the bias voltage. Furthermore, we can observe a new peak at −0.422 eV and −0.824 eV when applying the bias voltages of 1.0 V and 2.0 V, respectively. We focused particularly on the PDOS for the C 2p orbitals at each bias, as shown in Figs. 6(c) and (d). We can confirm that the total DOS are primarily dependent on the PDOS for the C 2p orbitals at the end of the complex, which provided a new gap state at a low energy level below the Fermi level. These new gap states also contribute to the electrical conduction under the bias voltages. However, the I–V curve reflects basically the intrinsic semiconducting properties [15].

We also calculated the bias dependency of the electrical conduction of the $Cp_5In_4^-$ complex between the gold electrodes. The current was about 10^{-4} μA. The total DOS at the Fermi level is dependent on the PDOS for C 2p orbital at the end of the complex. Furthermore, the electrical conduction would not be influenced by the C 2p electrons localized on Cp ring at the end of the complex. The tunneling effect virtually disappears due to the long distance between the left and the right electrodes.

4. Conclusion

We have examined the electronic properties and electron transport of the Cp–In complex with the DFT approach. The polymeric complex exhibited semiconducting properties. The $Cp_5In_4^-$ complex between the gold electrodes exhibited low electrical conduction. The $Cp_3In_2^-$ complex between the gold electrodes had a gap state at the Fermi level, and the electrons were concentrated on the Cp ring at the end of the complex. Although the gap state enhanced the electrical conduction between the gold electrodes because of the short distance between the left and the right electrodes, the electrical conduction is dependent on the intrinsic characteristics of the semiconducting properties of the polymeric complex. The strong tunneling effect would be suppressed in the Cp–In complexes.

References

[1] Tao, N. J. (2006). *Nat. Nanotechnol.*, *1*, 173.
[2] Aviram, A., & Ratner, M. A. (1974). *Chem. Phys. Lett.*, *29*, 277.
[3] Stokbro, K., Taylor, J., & Brandbyge, M. (2003). *J. Am. Chem. Soc.*, *125*, 3674.
[4] Staykov, A., Nozaki, D., & Yoshizawa, K. (2007). *J. Phys. Chem. C*, *111*, 11699.
[5] Brizuela, G., & Hoffmann, R. (1998). *J. Phys. Chem. A*, *102*, 9618.
[6] Matsuura, Y., & Uchimiya, R. (2010). *Solid State Commun.*, *150*, 1400.
[7] Zhou, L., Yang, S., Ng, M., Sullivan, M. B., Tan, V. B. C., & Shen, L. (2008). *J. Am. Chem. Soc.*, *130*, 4023.
[8] Yi, Z., Shen, X., Sun, L., Shen, Z., Hou, S., & Sanvito, S. (2010). *ACS Nano*, *4*, 2274.
[9] Jutzi, P., & Burford, N. (1999). *Chem. Rev.*, *99*, 969.
[10] Atomistix ToolKit 10.8.2; Quantumwise A/S, www.quantumwise.com
[11] Brandbyge, M., Mozos, J. L., Ordejon, P., Taylor, J., & Stokbro, K. (2002). *Phys. Rev. B*, *65*, 165401.
[12] Fürst, J. A., Brandbyge, M., Jauho, A., & Stokbro, K. (2008). *Phys. Rev. B*, *78*, 195405.
[13] Candell, E., Eisenstein, O., & Rubio, J. (1984). *Organometallics*, *3*, 759.
[14] Janiak, C., & Hoffmann, R. (1990). *J. Am. Chem. Soc.*, *112*, 5924.
[15] Ng, M., Shen, L., Zhou, L., Yang, S., & Tan, V. B. C. (2008). *Nano Lett.*, *11*, 3662.